Albatrosses employ orientation and routing strategies similar to yacht racers

Yusuke Goto[1]*, Henri Weimerskirch[2], Keiichi Fukaya[3], Ken Yoda[1], Masaru Naruoka[4], Katsufumi Sato[5]

[1]*Graduate School of Environmental Studies, Nagoya University, Furo, Chikusa, Nagoya, Japan.*

[2]*Centre d'Etudes Biologiques Chizé, CNRS – Université de la Rochelle, 79360 Villiers En Bois, France*

[3]*National Institute for Environmental Studies, Tsukuba, Ibaraki, Japan*

[4]*Aeronautical Technology Directorate, Japan Aerospace Exploration Agency, 6-13-1 Osawa, Mitaka, Tokyo, Japan*

[5]*Atmosphere and Ocean Research Institute, The University of Tokyo, Chiba, Japan.*

Author Contributions: YG, HW, KF, KY, MN and KS designed the study; HW collected data; YG analyzed the data; all authors participated in the writing of the manuscript (YG wrote the first draft).

Competing Interest Statement: The authors declare no competing interests.

Abstract

The way goal-oriented birds adjust their travel direction and route in response to the wind significantly affects their travel costs. This is expected to be particularly pronounced in albatrosses, which employ a wind-dependent flight style called dynamic soaring. Dynamic soaring birds in situations without a definite goal, e.g. searching for prey, are known to preferentially fly with tail-to-side winds to increase the speed and search area. However, little is known about their reaction to wind when heading to a definite goal, such as returning to their nest. For example, returning tracks of albatrosses vary from beelines to zigzags similar to that of sailboats; however, there is no empirical test of whether the wind causes this variation. Here, based on the similar wind-dependent speed between albatrosses and sailboats, we tested whether the time-minimizing strategies used by yacht racers can explain the locomotion patterns of wandering albatrosses. We predicted that when the goal is located upwind or downwind, albatrosses should (i) deviate their travel directions from the goal on the microscale and (ii) increase the number of turns on the macroscale. Both hypotheses were supported by track data from albatrosses and racing yachts in the Southern Ocean confirming that albatrosses qualitatively employ the same strategy as yacht racers. Nevertheless, albatrosses did not strictly minimize their travel time, likely making their flight robust against wind fluctuations. Our study provides the first empirical evidence of tacking in albatrosses and demonstrates that man-made movement strategies provide a new perspective on the laws underlying wildlife movement.

Introduction

Birds routinely traverse great distances to reach their destination. Some species partake in globe-spanning migrations from their wintering spot to their breeding grounds (1, 2), and some species repeat long-distance foraging trips during the breeding season, foraging hundreds or thousands of kilometers from their nests and returning to feed their chicks (3, 4). Their routinal long-distance flights entail enormous travel cost, such as energy and time. Wind is an environmental factor that significantly impacts this cost; tailwinds increase the travel speed of birds, headwinds slow them down, and crosswinds can divert them from their intended route (5–7). Therefore, through natural selection, birds are expected to have acquired a navigational capacity that allow them to select efficient, travel cost-saving routes under any wind conditions they may encounter (8–10). This macro-scale route selection consists of a series of decisions pertaining to the travel direction in response to the goal and wind directions (called orientation) (6). The orientation is expected to be further influenced by microscopic flight dynamics, i.e., how energy and time required to travel unit distance varies depending on the travel direction relative to the goal and wind directions (11, 12). To better understand the birds' hierarchically structured navigation in wind flow, it is imperative to predict their orientation and route selection based on micro-scale flight dynamics and to test predictions using real data (12). Although bird orientation and route selection based on the wind has been extensively investigated at a coarse scale, empirical studies on how microscopic flight dynamics shape orientation and route selection are lacking.

Among the spectacular journeys exhibited by various bird species, those of procellariform seabirds (i.e., petrels, shearwaters, and albatrosses) are one of the most distinctive because of their underlying wind-utilizing flight style and may thus provide excellent opportunities to test the implications of micro-scale flight dynamics to orientation and route selection in response to the wind. These pelagic seabirds fly several hundreds or thousands of kilometers away from their nests during their breeding period (3, 4). During these foraging trips, the birds flap their wings for only a small fraction of their flight time (e.g., 1–15% for wandering albatrosses (13)). This efficient travel strategy is enabled by their flight style, called dynamic soaring, in which the birds can harvest aerodynamic kinetic energy from the atmosphere by utilizing wind speeds that increase with the altitude above the sea surface (14–16). This wind-dependent flight dynamic creates a dependence on wind-direction for travel speed and energy consumption rate (17–19), and may thus affect orientation and route selection. However, despite the numerous tracking studies on procellariiform seabirds over the last three decades (20–22), the orientation and route selection of the birds heading to their goals remain largely unexplored.

To elucidate the navigation strategies of goal-directed birds in wind, it is necessary to study their movements in relation to not only wind direction but also goal direction (6), which requires us to define the bird's goal location in the first place. Many studies have shown that procellariiform seabirds prefer tail-to-side winds during their foraging trips (17, 23–27); yet, these studies have not focused on situations in which the bird’s goal is defined. Foraging trips of pelagic seabirds, like those of other central place foragers (28), are often categorized into three phases: outbound, middle, and returning (29). In the outbound and middle phases, there are no goal locations, or, if any, are large areas with a scale of several hundred kilometers, such as a frontal zone (30), while the nest is a definite goal in the returning phase. Hence, the factors that constrain bird behavior are distinctly different between the returning and non-returning (outbound and middle) phases. In the non-returning phase, the constraint to reach the goal is weak or absent, and the bird is expected to prioritize maximizing speed and consequently, the search area. By contrast, in the returning phase, the priority is reaching the goal with less travel cost by simultaneously taking the wind and goal direction into account. Previous studies on procellariiform seabirds examined their travel direction relative to wind direction throughout their entire trip, without distinguishing the returning and non-returning phases (17, 23–27). Thus, while the tail-to-side wind preferences of dynamic soaring birds reported in these studies are consistent with predictions of maximizing prey-searching efficiency in the non-returning phase, they do not provide insights into navigation strategies in the returning phase as they did not take goal direction into account. Although returning and non-returning have been analyzed separately in some studies (29, 31), the focus has only been on the birds’ travel directions relative to the wind direction. Thus, there is little information on how the goal-oriented procellariiform seabirds adjusts its movement in response wind direction in relation to the goal direction. Moreover, we re-examined the returning portion of previously published albatross track data (32, 33) and found that their returning tracks show a variety of patterns ranging from beeline to zigzag like a sailboat (Fig. 1); however, whether this diversity in flying patterns can be explained by variation in the wind direction relative to the goal has not been verified as yet.

In this study, we examined the orientation and route selection of yacht racers, who’s speed is wind-direction dependent, similar to that of procellariiform seabirds, to help elucidate the dynamics of soaring birds in returning. The kinetic mechanism of sailing maximizes the speed of a sailboat in a crosswind and reduces it in tailwind and headwind (34). Due to this wind-direction dependence of travel speed, yacht racers are known to orient their course away from the goal when the goal is located leeward or windward in order to reach the goal faster, resulting in a zigzag route at the macro-scale, called “tacking” (34, 35). Recent theoretical studies have reported that the kinetic mechanism that harvests energy from the wind in dynamic soaring is similar to that of sailing (16). Another study reported that wandering albatrosses show wind-direction dependence of travel speed, similar to that of sailboats (19). If albatrosses are expected to try to minimize energy expenditure to reach their goal, and if we can assume that elapsed time is a good approximation of energy expenditure (this assumption is discussed in more detail in **Results**), we can derive the hypothesis that albatrosses returning to their nests use a time-minimizing strategy similar to that of sailboat racers. One of the difficulties in testing this hypothesis is the need to examine the travel speed of albatrosses in various wind directions, as well as the travel direction of returning albatrosses in various wind conditions for various goal directions in detail , which requires a large amount of high-resolution tracking data, and not lowresolution data (such as satellite tracking data with sampling intervals of several hours used in some studies; (17, 19, 26, 29)).

In the present study, we tested whether the time-minimizing strategies used by yacht racers can explain the locomotion patterns of wandering albatrosses using large amount of tracking data of their foraging trip during the incubation period (149 tracks consisting of 407,659 data points in total) recorded at high sampling interval (1 data point every 2 min). We predicted that when the goal is located upwind or downwind, albatrosses should (i) deviate their travel directions from the goal at the microscale and (ii) increase the number of turns at the macroscale. We tested these predictions with tracking data from albatrosses and racing yachts in the Southern Ocean.

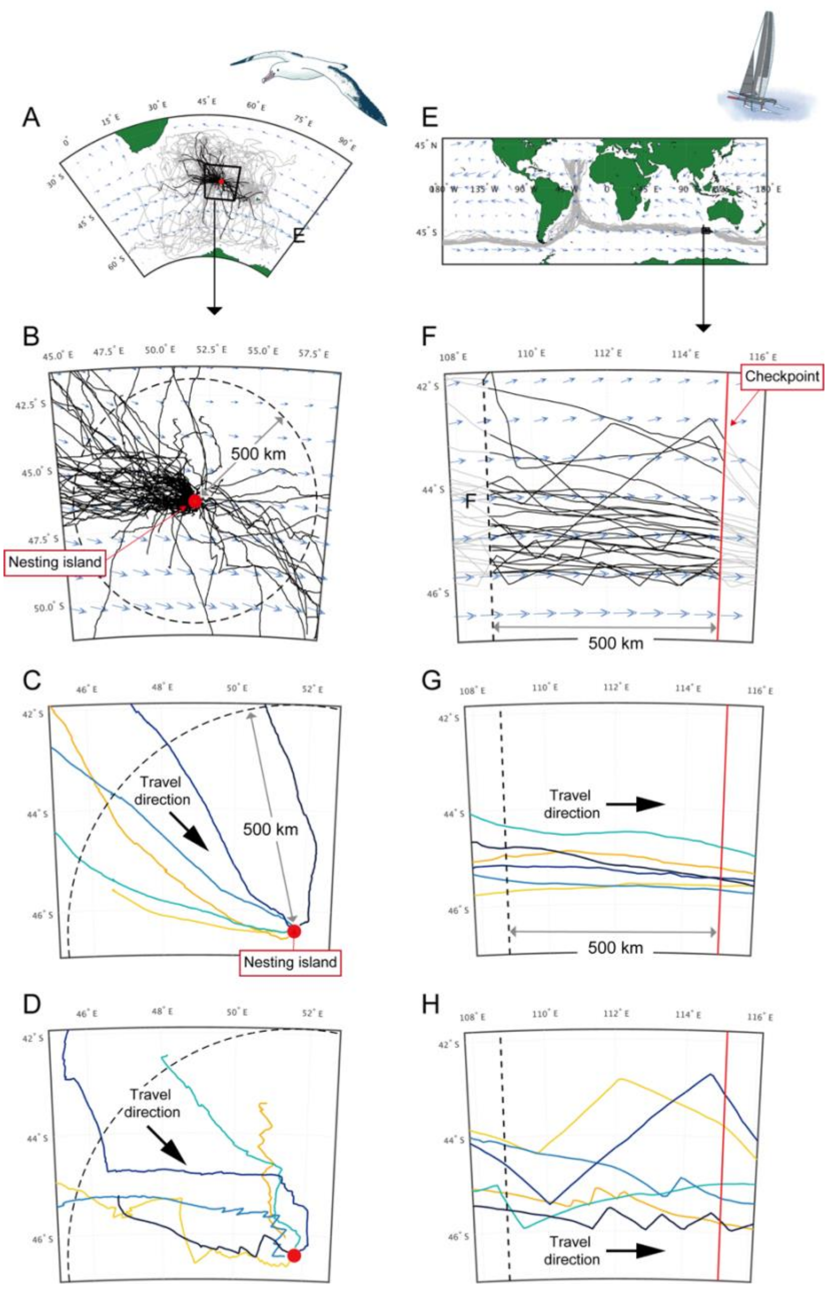

Fig. 1 Tracks of albatrosses and racing sailboats. (A) Foraging trips of wandering albatrosses recorded by GPS (*N* = 149). Portions of tracks in returning phase are shown in black lines and the other portions are shown in grey lines. (B) Returning tracks of albatrosses within 500 km from the nesting island (Possession Island). Light blue arrows in (A–B) represent average winds for January 2018 based on ERA5 ECMWF.(C–D) Returning tracks of albatrosses in straight lines (C) and winding patterns (D). (E) Tracks of sailboats in the 2020 Vendée Globe race around the world. (F) Tracks (black lines) of sailboats within 500 km from the middle checkpoint (red line). Light blue arrows in (E–F) represent average winds for December 2020 based on ERA5 ECMWF. (G–H) Tracks of sailboats within 500 km from the middle checkpoint in straight lines (G) and winding patterns (H).

Results

First, we confirmed the similarities in wind-dependent travel speeds between sailboats and albatrosses (19). Thereafter, we derived predictions of albatross movement based on the time-minimizing orientation strategies used by sailors. Then, we tested these predictions qualitatively and quantitatively by using track data of albatross and sailboats.

Similarities in wind-dependent travel speeds between sailboats and albatrosses

We analyzed track data (1 data point every 2 min) from 149 foraging trips made by wandering albatrosses during their breeding period from Possession Island, Crozet Islands, and track data (1 data point every 30 min) from 28 yachts participating in the 2020 “Vendée Globe”, a non-stop round-the-world yacht race across the Southern Ocean (Fig. 1). Both albatrosses and sailboats mainly traveled in 40–60°S latitudes and were constantly exposed to strong winds (average wind speed was 8.7 ± 3.4 m s^{-1} for albatross and 8.1 ± 3.0 m s^{-1} for sailboats).

We calculated the speed and direction of the albatross and yacht by computing a vector connecting two successive data points (N = 407,659 for albatrosses and N = 102,922 for sailboats); the average distances traveled between the two observation points by the albatrosses and sailboats were 1.49 ± 0.62 km and 12.1 ± 3.4 km, respectively. Consequently, the average travel speed was 12.4 ± 5.2 m s^{-1} for albatrosses and 6.7 ± 1.9 m s^{-1} for sailboats. Their travel speed changed according to the travel direction relative to the wind direction (Fig. 2). Such plots are called “polar diagrams” in the field of sailing. In theory, the speed of sailboats decreases in tailwinds and headwinds, thereby creating butterfly-shaped polar diagrams (34). A recent study reported that the polar diagrams of wandering albatrosses were also butterfly-shaped, based on track data at 1 h sampling intervals (19). We confirmed the butterfly-shaped polar diagrams of the sailboats and albatrosses in our data by fitting non-parametric functions (see **Methods**). As described below, these butterfly-shaped polar diagrams are expected to shape the movement strategies of both the yacht racers and albatrosses.

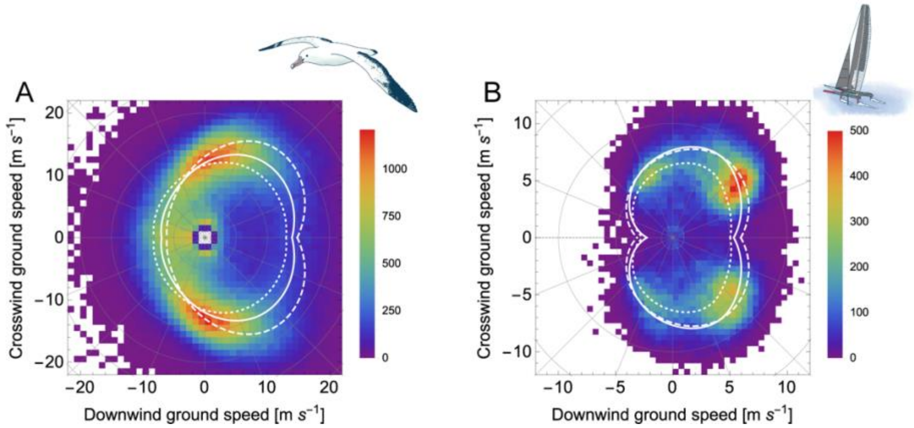

Fig. 2 Similarities in wind-dependent travel speeds between sailboats and albatrosses. Two-dimensional histogram of the ground velocity of albatrosses (A) and sailboats (B). Histograms in bins of 1 m s^{-1} for albatrosses and 0.5 m s^{-1} for sailboats. Colors represent the number of data points in each bin. The white lines indicate polar diagrams obtained by applying the general additive models (GAM) to the data. The solid line shows the polar diagrams with a 9 m s^{-1} wind speed, dotted lines with 6 m s^{-1} wind speed, and dashed lines with 12 m s^{-1} wind speed.

Prediction of albatross movement based on time-minimizing orientation strategy by sailors

We focused on a situation in which sailboat racers and albatrosses targeted defined goals, i.e. an intermediate check line south of Australia for sailboats and a nesting island for birds, respectively (Fig. 1). Their decision-making may be influenced by multiple factors including wind-dependent speed (19) and energy expenditure (17), the spatiotemporal pattern of wind conditions, and the prediction of wind conditions to the goal. In this study, we assumed that 1) albatrosses and yacht racers decide on their travel direction based on the local wind at their position and 2) that yacht racers and the albatrosses would try to minimize their elapsed time to reach their respective goals. The second assumption is obviously true for racing yachts but would also apply to albatrosses for two reasons. First, an earlier return to the nest would reduce the risk of nest abandonment by the partner protecting the eggs or chicks (36, 37). The second reason is that minimizing energy expenditure during travel should be advantageous to the survival and reproduction of wandering albatrosses, as for other animals (38). The consumed energy per unit distance traveled is proportional to elapsed time if the dependence of energy consumption rate on travel direction relative to wind is negligibly small. Hence, elapsed time is a good metric for energy consumption, and thus minimizing travel time leads to minimizing consumed energy (We will discuss the validity of this assumption in Discussion).

Under these assumptions, we derived two hypotheses from the maximum VMC (Velocity Made good on Course) strategy—a basic sailing strategy wherein the sailboats travel in the direction that maximizes the VMC, i.e., the parallel component of the velocity to the goal (Fig. 3A) (35). When the crosswind is blowing against the goal, the maximum VMC direction is approximately in line with the goal direction (Fig. 3B). In contrast, when the goal is located downwind (leeward) or upwind (windward), two maximum VMC directions deviate from the goal (Fig. 3B). This orientation also affects large-scale movement (Fig. 3C). In a crosswind, the route to maximize VMC will be a straight line. When the goal is located downwind or upwind, the traveler should alternatively switch travel directions (called “tacking” in sailing), resulting in zigzag track patterns. Note that, if the wind is steady and tacking is not costly, there is flexibility in the frequency of tacking, i.e., the size of the zigzag.

To summarize our hypotheses, when the goal is located downwind or upwind, yacht racers and albatrosses employing a maximum VMC strategy would deviate their travel direction from the goal (hypothesis 1) and increase the number of turns (hypothesis 2) compared to when the crosswind is blowing against the goal.

Qualitatively similar movement patterns between albatrosses and sailboats

To test these hypotheses, we analyzed the tracks of sailboats and albatrosses. The Vendée Globe has several checkpoints that racers must pass on the way, with the 115°08'09"E longitude line of Cape Leeuwin being one of them and hereafter referred to as the “finish line”. We used the tracks of sailboats within 500 km from the finish line (Fig. 1F). For albatrosses, we used the portion of their tracks returning to and within 500 km from the nesting island (Fig. 1B).

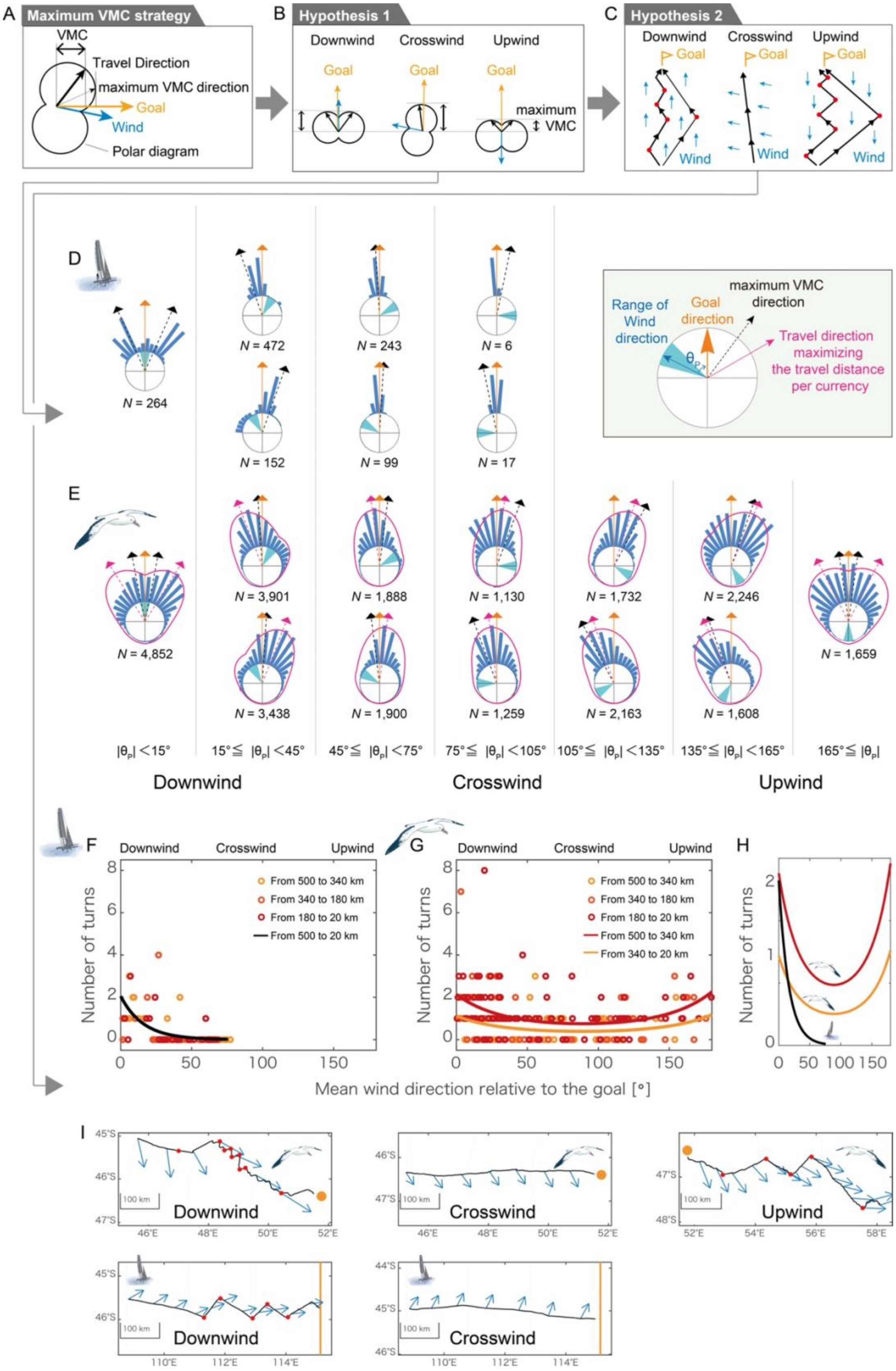
A
Maximum VMC strategy
VMC
Travel Direction
maximum VMC direction
Goal
Wind
Polar diagram
B
Hypothesis 1
Downwind
Crosswind
Upwind
Goal
Goal
Goal
maximum
VMC
C
Hypothesis 2
Downwind
Crosswind
Upwind
Goal
Goal
Goal
Wind
Wind
Wind
D
N = 264
N = 472
N = 152
N = 243
N = 99
N = 6
N = 17
Range of Wind direction
Goal direction
maximum VMC direction
Travel direction maximizing the travel distance per currency
θp
E
N = 4,852
N = 3,901
N = 3,438
N = 1,888
N = 1,900
N = 1,130
N = 1,259
N = 1,732
N = 2,163
N = 2,246
N = 1,608
N = 1,659
|θp| <15°
15°≦ |θp| <45°
45°≦ |θp| <75°
75°≦ |θp| <105°
105°≦ |θp| <135°
135°≦ |θp| <165°
165°≦ |θp|
Downwind
Crosswind
Upwind
F
Downwind
Crosswind
Upwind
Number of turns
From 500 to 340 km
From 340 to 180 km
From 180 to 20 km
From 500 to 20 km
0
2
4
6
8
0
50
100
150
G
Downwind
Crosswind
Upwind
Number of turns
From 500 to 340 km
From 340 to 180 km
From 180 to 20 km
From 500 to 340 km
From 340 to 20 km
0
2
4
6
8
0
50
100
150
H
Number of turns
0
1
2
0
50
100
150
Mean wind direction relative to the goal [°]
I
45°S
46°S
47°S
46°E
48°E
50°E
52°E
100 km
Downwind
46°S
47°S
46°E
48°E
50°E
52°E
100 km
Crosswind
47°S
48°S
52°E
54°E
56°E
58°E
100 km
Upwind
45°S
46°S
110°E
112°E
114°E
100 km
Downwind
44°S
45°S
46°S
110°E
112°E
114°E
100 km
Crosswind

Fig. 3 Prediction of albatross movement based on time-minimizing orientation strategy by sailors and test in track data. (A) Definition of velocity made course (VMC). (B) Travel directions that maximize VMC for each wind condition. Blue arrows indicate wind direction, orange arrows indicate the goal direction, and black arrows indicate travel directions that maximize the VMC. (C) Macroscale travel patterns predicted from the maximum VMC strategy. Red points represent turning points. (D–E) Histograms of the travel direction of sailboats (D) and albatrosses (E) relative to the goal direction. Each row indicates the different wind directions relative to the goal direction. The histograms are generated from the track data in Fig. 1 (within 500 km from the finish line or nesting island). The orange arrows indicate the goal direction. The cyan fans indicate the range of wind directions. The black arrows indicate the maximum VMC direction. For the albatrosses, the travel directions that maximize the travel distance along the goal per currency are shown with pink arrows. In addition, the fitted probability distribution of our stochastic model (see Methods for detail) is shown by pink lines. (F–G) The number of turns in response to wind direction relative to the goal for sailboats (F) and albatrosses (G). (H) The fitted line of data in (F) and (G). Albatrosses evidently made more turns than sailboats. (I) Example of tracks (black solid lines) of albatrosses (upper row) and sailboats (lower row) within 500 km from their goals. The orange dots in the upper row represent the nesting island of birds. The orange line in the lower row shows the finish line (one of the middle checkpoints of the race corresponding to the longitude of Cape Leeuwin). The blue arrows represent the wind direction on the track. The red points represent the identified turning points. When the goal was located downwind and upwind (first and third column), more turns occurred compared to the crosswind condition (the second column).

The data supported the first hypothesis. Fig. 3D and E show histograms of the travel direction with different wind directions to the goal. These travel directions are every 2 min (1.49 ± 0.62 km in distance, N = 27,776) for albatrosses and every 30 min (12.1 ± 3.4 km in distance, N = 1,253) for sailboats. The peaks of the travel direction of sailboats and albatrosses both deviated from the goal when the goal was located downwind (and upwind for albatrosses).

The data also supported the second hypothesis. We defined a meander with >10 km width as one turn. Then, we counted the number of turns for three sections according to the distance from the goal (500–340 km, 340–180 km, and 180–20 km). The average wind direction of each section was also determined. We obtained 226 sections from 95 tracks for albatrosses and 84 sections from 28 tracks for sailboats (See **Methods** for details). The number of turns increased significantly with the downwind goal for both sailboats and albatrosses and with the upwind goal for albatrosses (Fig. 3F–H and Table S1–S2). Examples of zigzag patterned tracks in downwind and upwind goals, as well as those of straight patterned tracks in crosswind goals, are shown in Fig. 3I. All tracks are shown in Fig. S2–S7.

Quantitative difference between movement patterns of albatrosses and sailboats

While our analysis showed qualitative similarities between the movement patterns of albatrosses and yacht racers, it also implied some quantitative differences that were further examined as follows.

(i) Deviation from time minimization as primary travel currency

The travel direction of albatrosses slightly deviated from the optimal time-minimizing flight directions (black arrows in Fig. 3E). This discrepancy indicates that, for albatross in returning, time is not the only “currency of travel” (i.e., the variable albatrosses tried to minimize during their travel). In this regard, energy might be the true currency of travel. For instance, as not only the travel speed but also the energy consumption rate depends on the wind direction in wandering albatrosses (17), preferred travel directions are expected to differ based on whether time or energy is being minimized, which might explain this observed discrepancy. Alternatively, the currency might be a combination of time and some unexpected factors.

To quantify the deviation from the time minimization prediction and explore the characteristics of the currency albatross employed, we constructed a stochastic movement model (see **Methods**). Our model assumes a bird moves with a higher probability in the travel direction, which results in a greater travel distance along the goal direction per consumed currency. This probability is governed by how the travel speed and the currency consumption rate (CCR; i.e., currency consumed per time) vary depending on the travel direction of the bird. If the currency is time (e.g., maximum VMC strategy), the CCR does not depend on the travel direction. If the currency is energy, the CCR should increase in the headwind based on the observed heart rate pattern (17). Furthermore, we can obtain insights into the characteristics of unforeseen factors in currency by testing the CCR functions that would better explain the data.

Here, we employed three CCR functions in which the travel direction is a variable. Though simplified, these capture the features of potential currencies: constant (assumed currency: time), linear (assumed currency: energy), and quadratic (assumed currency: unknown). Models assuming each function were applied to the track direction data (Fig. 3E), and the quadratic function model was selected based on the Bayesian information criterion (BIC), i.e. the CCR increased with headwind and tailwind (Fig. 4A and Table S3). This result indicates that the travel currency is not exactly time or energy.

Overall, although time can be regarded to be the main currency as it well explained the qualitative movement patterns of albatrosses, the quantitative analysis indicated that additional factors should be included in the currency (Potential factors are explained in further detail in the **Discussion)**.

(ii) Difference in frequency of large-scale turns

There were qualitative differences in the frequency of turns in large-scale movement (Fig. 3H). Firstly, turns occurred more frequently for albatrosses than for sailboats. Secondly, the frequency of the occurrence of turns was independent of the distance to the goal for the yacht, whereas albatrosses had a predominantly higher frequency of turns when the goal was closer (340–20 km) than when it was farther away (500–340 km. See Table S1–2).

Discussion

This is the first study to compare the track data of wandering albatrosses and sailboats, and the results of our study determined that wandering albatrosses and sailboats show similar orientation and routing when heading to their goals, along with some quantitative differences.

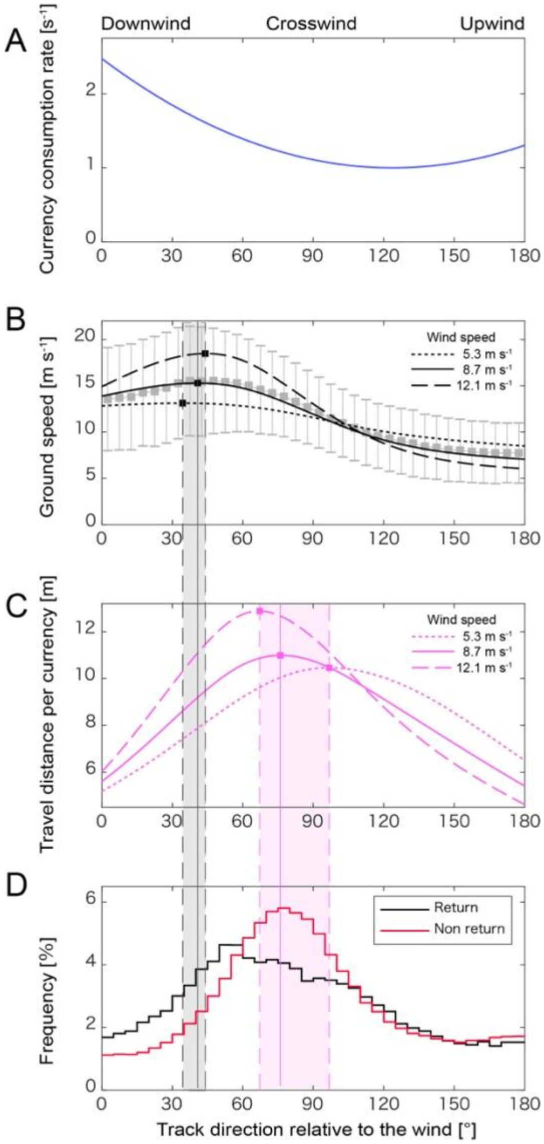

Fig. 4 Travel direction of albatrosses deviates from the speed maximizing direction. (A) Estimated cost consumption rate function, $C(\theta_G) = 1 + 0.314(|\theta_G| - 2.18)^2$. The horizontal axis represents the travel direction relative to the wind. (B) The mean and standard deviation values of the ground speed of wandering albatrosses for all tracks are shown for each 5° of travel direction relative to the wind. The black lines correspond to the polar diagram in Fig. 2. The solid black line represents a wind speed of 8.7 m s^{-1} (the mean wind speed experienced by the albatross), the dotted line of 5.3 m s^{-1}, and the dashed line of 12.1 m s^{-1} (mean wind speed ± standard deviation). The black squares represent the travel directions achieving the maximum ground speed for each wind speed. (C) The distance an albatross can travel per currency at a wind speed of 8.6 m s^{-1} (solid line), 5.3 m s^{-1} (dotted line), and 12.1 m s^{-1} (dashed line). These lines are obtained by dividing the polar diagrams in (B) with the cost function in (A). The maximum value is obtained when the travel direction of the bird to the wind is 83°. (D) Histogram of the travel direction relative to the wind for wandering albatrosses in the non-returning (orange, *N* = 374,969) and returning (right blue *N* = 47,839) phase. The grey zone on panel B-D, indicates range of the travel directions achieving the maximum ground speed at wind speed from 5.3 m s^{-1} to 12.1 m s^{-1}. The pink zone on panel C-D, indicates range of the travel directions maximizing travel distance per the currency. The peak of the frequency distribution of the travel direction to the wind is out of the gray zone, but well within the pink zone.

Qualitative findings: albatrosses show similar orientation as sailboats and “tacking”

The way birds adjust their travel direction in response to the wind directions relative to their goal directions is fundamental information for understanding the movement strategies of birds (6). However, in dynamic soaring birds, the relationship between these three directions (i.e., the travel direction of the bird, wind direction, and goal direction) has rarely been explored. Although previous studies reported that dynamic soaring birds preferentially fly with tail-to-side winds (17, 23, 24, 26, 27, 29), these studies only explored the relationship between the wind direction and the travel direction of the bird. Here, we showed that albatrosses flexibly adjust their travel direction according to “the wind direction relative to the goal direction”. Albatrosses, like sailboats, deviate their travel direction from leeward and windward goals in small-scale (1–2 km) movements and switch travel direction more frequently when the goal is located upwind or downwind in large-scale (>10 km) movements (similar to tacking in sailing), and some tracks showed clear zigzag patterns. Note that this large-scale zigzag is different from the well-known several-100 m-scale zigzag pattern which stems from the S-shape track of one cycle of dynamic soaring (39–41).

To the best of our knowledge, this is the first empirical verification that albatrosses adjust their direction of movement in response to wind direction similar to sailboat racers. Two studies (25, 40) have reported that tracks of albatross proceeding upwind exhibit zigzags at 100 m to 1 km scales, and this phenomenon was discussed using yacht tacking as an analogy (19, 40) (yet, these discussions were based on data arbitrarily selected from the entire available data sets, and the total length of these selected tracks is less than 20 km even when the two studies were combined). In addition, a recent study (27) reported "zigzag flights" in the dynamic soaring birds, the blue petrels. The blue petrels made a series of approximately 180° turns during their foraging trips. This zigzag was explained by their crosswind preference for efficient prey search. However, because these studies (19, 27, 40) were conducted in situations where the animal's goal was not clearly defined, it was unclear whether the bird's turn was caused by the wind. Our study focused exclusively on situations in which the goal was clearly defined (i.e. returning), allowing us to systematically examine how the flight direction and number of zigzag turns of albatrosses vary with the wind direction relative to the goal. Consequently, we were able to provide the first experimental evidence that albatrosses turn with wind, i.e., evidence of tacking in albatrosses.

Quantitative findings

(i) Albatrosses make more turns than sailboats

We found that albatrosses made turns more frequently than sailboats. This may reflect on the cost of turning for sailboats and albatrosses. In sailboats, turns require changing the direction of the sail, and, in the Vendée Globe race, only one person is allowed on the sailboat, so turns could be more costly in terms of both time and energy than for albatrosses. As a result, it is expected that a strategy to reduce the number of turns is adopted in yacht races.

We also found that the number of turns increased as albatrosses approached their goals, but it did not increase for sailboats. This may reflect the difference in their goals; in sailboats, the goal is a line, while in albatrosses, it is a point. Therefore, albatrosses may make more turns to fine-tune their travel direction when they are close to the goal.

(ii) Albatrosses do not maximize their speed

We found that the travel currency for returning albatrosses is not time alone. This finding challenges the conventional idea that dynamic soaring birds prefer crosswinds to maximize their travel speed (17, 26).

Previous studies have indicated that the currency of travel is time for wandering albatrosses. Since albatrosses capture prey that are randomly and widely distributed, maximizing the prey encounter probability should be prioritized during prey search (i.e., the non-returning phase), and thus albatrosses are expected to prefer the direction that maximizes the travel distance per currency. The previous study showed that wandering albatrosses prefer the speed-maximizing direction during the entire foraging trip(17), thus, indicating that time is the currency of their travel. Similar results have also been reported for another dynamic soaring species, Gadfly petrels (26).

However, our results suggested that time was not the currency in the “returning” of wandering albatrosses. Two possible hypotheses consistently explain our findings and that of previous studies. First, time is the travel currency during non-returning (previous studies) but not during returning (our results). Second, the currency is not time, even during non-returning. As previous studies used tracking data of 1- to 2-h sampling intervals (17, 26), the coarse temporal resolution may have obscured the small-scale movement patterns.

Using our data (2-min intervals), we calculated the travel direction of albatrosses during non-returning (Fig. 4D), which did not match the speed maximizing direction (black lines from Fig. 4B), unlike that in the previous studies, thus supporting the hypothesis that time is not the travel currency of wandering albatross even during non-returning. Meanwhile, the peak of the travel direction during non-returning matched well with the travel direction that maximizes the travel distance per the currency that albatrosses employed during “returning” (pink lines from Fig. 4C). Thus, our results suggest that time is not the travel currency of albatross even during non-returning.

Speed or robustness: Which will be the priority for the dynamic soaring birds in fluctuating winds?

The next question to address is what the additional factor in the currency (Fig. 4A and D) could be. Although it cannot be identified from the present results alone, a potential candidate currency is the risk-aversion of costly flapping flights. Soaring birds are spared from flapping flight by exploiting the energy from wind. However, wind conditions are unpredictable and dynamic, which may necessitate birds to conduct flapping flights, which is known to be very costly. Hence, for soaring flight, not only speed but also the robustness to stochastic changes in the winds should be key factors, whereby birds try to minimize the duration of flapping flight. This is particularly important for the largest species like wandering albatrosses which apart from taking off, use flapping flight extremely rarely (13).

This risk-aversion strategy is already known in thermal soaring birds (42–44). Thermal soaring is a flight style in which birds repeatedly ascend with updrafts (convection currents) and then glide. If the bird knows the distance and updraft speed of successive thermals, the theory predicts an "optimal speed" that maximizes horizontal travel speed (45, 46). However, in practice, large bird species employ a slower airspeed than this “optimal speed” (42). The slower airspeed allows them to traverse long distances with less descent in altitude. In this manner, birds can reduce the risk of not finding the next thermal because of its stochastic distribution and thus being forced to perform flapping flights (42).

Our results may indicate that dynamic soaring species also employ a risk-aversion strategy. In the theory of dynamic soaring, the wind gradient is often simplified to be invariant in time and space, except in the altitude (16, 47, 48). However, real wind gradients are turbulent and fluctuate spatiotemporally (49). This uncertainty of the wind may force the albatross to prioritize wind energy harvesting efficiency. At a small scale, the energy harvested from wind gradients by dynamic soaring increases when the direction of bird flight is aligned upwind when the bird is ascending and downwind when the bird is descending (15, 16, 31). Accordingly prioritizing speed reduces the time to satisfy this condition and compromises the energy harvesting efficiency. Therefore, a strategy that maximizes speed would have, compared to a strategy that prioritizes energy harvesting efficiency, a higher risk of failing to exploit energy and being forced into costly flapping flights when the bird experiences unexpected fluctuations in the wind. To avoid this risk, wandering albatrosses may have favored travel directions that prioritize energy-harvesting efficiency, despite their slower speeds. A recent study reported that Manx shearwaters, which use both dynamic soaring and flapping flight, prefer energy harvesting efficient travel (31). In future work, testing the energy-harvesting efficiency prioritizing hypothesis using detailed tracking data of wandering albatrosses, specialists of dynamic soaring, would be an intriguing prospect.

Navigation strategies of yacht racers provide a new perspective on seabird navigation

Pelagic seabirds are a unique group in the animal kingdom with the richest accumulation of track data (22, 50–52). As demonstrated in this study, leveraging the knowledge of sailboat racers and engineers can be a powerful tool to uncover this vast data and determine the underlying rules that govern the motion of pelagic seabirds. For example, although our study made the simplification that albatrosses choose their travel direction based solely on local wind direction, birds may perceive or empirically predict a wide range of wind environments and determine their travel direction based on these (17, 26, 27). Autonomous sailing algorithms should be applied to examine these more complex movement strategies (53, 54). These algorithms determine the feasible travel direction by taking into account not only the goal location, real-time local-scale wind measurements, and the polar diagram of the sailboat, but also global-scale wind predictions and tacking costs (53, 54). Appropriating these algorithmic formulations to the study of dynamic soaring bird travel should help reveal the currency of travel and the cognition capability of these birds, which would be an interesting future challenge.

Methods

Track data

We used the track data of wandering albatrosses from 2003–2005 and 2016–2019 collected in previous studies (32, 33) (Fig. 1A–D). All data were obtained from breeding individuals on Possession Island (46°25'S. 51°45'E). Portions of tracks within 20 km of the Island were excluded from the analysis to avoid the influence of land. Trips of incomplete recordings that stopped before the nest was reached were excluded from the analysis. In total, we obtained data for 149 foraging trips. An iterative forward/backward averaging filter was applied to each track to exclude unrealistic points with speeds of more than 100 km h^{-1}. Furthermore, since sampling intervals differed among the data (10 s to 2 min), the data were resampled every 2 min.

Additionally, data from the Vendée Globe, a long-distance yacht race held in 2020, was used for sailboats (Fig. 1E–H). Of the participating boats, we used data from 28 boats that passed through the middle checkpoint (longitude 115°08'09"E line). For the analysis, we used the route below a latitude of 30 degrees north. The positions of all the boats were recorded every 30 min.

Defining the returning phase of wandering albatross

We identified the returning start points for each albatross track. The portion of tracks after the returning start point was defined as the returning phase, while that prior to the start point was defined as the non-returning phase. We employed a backward path analysis to determine the returning start point (55, 56). In this method, by starting at the goal location and moving backward along the path, the backward beeline distance (*BD*) and the backward path length (*BL*) were calculated for each point. The point at which *BD* stopped increasing linearly with respect to *BL* was defined as a returning starting point. Although previous studies visually determined the point of change from linear to non-linear, in this study, we defined the returning starting point using the following procedure to ensure reproducibility. First, we calculated the *BD* and *BL* for each point. The *BL* and *BD* data set was then resampled to record BL for every 10 km. We then applied a 50 km moving average to the *BL*. Subsequently, *BD* was plotted against *BL*, and the peak points of *BD* were detected. Among these peaks, point *P* with the smallest *BL* was determined. In the *BD* vs. *BL* plot, a linear and broken line with one change point was respectively fitted to the region where $BL \leq P$, and the BIC were calculated for the two. If the broken line showed a lower BIC than the linear line, and the slope of the line that was further away from the nest was less than half of the slope of the line that was closer to the nest, the position corresponding to the change point of the broken line was determined as the returning start point. In all other cases, the position corresponding to point *P* was determined to be the returning start point.

Calculation of ground velocity vector, wind vector, and goal direction

For each data point, we calculated (i) the ground velocity vector (travel direction and speed to the ground) and (ii) wind direction and wind speed. In addition, for data points in the returning phase and within 500 km of the goal, we also calculated (iii) the direction of the goal as follows.

(i) Ground velocity (ground speed and travel direction)

The ground velocity was calculated for each position by dividing the vector connecting two consecutive data points by the elapsed time. Since there were some instances of recording deficit, the ground velocity was not calculated for data points corresponding to these deficits; i.e., the ground velocity vectors were calculated only when there was a pre-resampling data point within 2 min before and after the two consecutive post-resampling data points. The track data included data when the albatross was flying at the sea surface. Therefore, albatross data points with a speed of less than 2 m s^{-1} were regarded as data points during their stay at the sea surface and were excluded from the analysis.

(ii) Wind direction and speed

For the wind direction and speed data, we used ERA5 ECMWF, hourly on a 0.25° grid (https://cds.climate.copernicus.eu/cdsapp#!/dataset/reanalysis-era5-single-levels?tab=overview). For each track data point, the estimates of wind direction and speed predictions at the closest point in time and distance were used.

(iii) Goal direction

The direction of the goal from the bird or sailboat was calculated for each data point for data within 500 km from the goal in the returning part of albatrosses and within 500 km from the finish line of the sailboat. For the albatrosses, the goal direction was calculated from GPS observation points, setting Possession Island as the goal, and for the sailboats, the goal direction was set to due east.

Identification of polar diagram using GAM

Based on the ground velocity vector and the wind vector obtained in the previous section, the polar diagrams of the albatrosses and sailboats were determined using a generalized additive model (GAM), a non-parametric smoother method (57). The ground speed (*V*) was used as the response variable, and the absolute value of the direction of movement relative to the wind (difference between the direction of ground velocity, i.e., travel direction, and the wind direction: θ_G) and the wind speed (*w*) were the explanatory variables. The calculations were performed in R v3.6.3 with the “gam” function of the “mgcv” package. We employed the “te()” function setting the tensor product smooths for the model formula (57). From these, the ground speed was obtained as a function of the direction of movement and wind speed relative to the wind, i.e., $V_G(\theta_G, w)$, and the polar diagram was obtained by displaying this function in polar coordinates.

Counting turns in tracks

To quantify the number of large-scale turns (>10 km wide), we applied the following procedure to portions of track data from sailboats and albatrosses within 500 km and >20 km from their goals.

(1) For distances less than *x* = 500, 420, 340, 260, or 180 km, at which the albatrosses started returning.

1-1: A point of track *x* km from the goal was selected as well as a point at (*x*–160) km from the goal, and a beeline was drawn by connecting these two points (Fig. S1A).

1-2: A time series of the **PDB** (Perpendicular Distance of the position of the traveler from the Beeline) was computed for points from *x* to (x-160) km from the goal point (Fig. S1B). The PDB was defined as positive when the traveler was on the left side of the beeline and negative when the traveler was on the right side.

When the track is straight, the PDB does not show a clear peak. In contrast, when the track is zigzag, PDB shows a distinct peak. The number of peaks in the PDB time series corresponds to the number of turns, and the degree of change represents the width of the zigzag pattern. Therefore, in this study, we detected the large-scale turns from the PDB. Specifically, we performed the following two procedures.

(2) For each PDB time series obtained in (1), the peaks with a prominence of 10 km or more were calculated at the bottom (blue points in Fig. S1C–D) and top (green points in Fig. S1C–D). The prominence of a peak is an index to quantify how much a peak stands out from the surrounding baseline of the signal, and is defined as the vertical distance between the peak and its lowest contour line. The “findpeaks” function in MATLAB v2019a was used to detect the peaks.

(3) For the detected peaks, if there were consecutive peaks with the same side (top-top or bottom-bottom), the one with the highest absolute value of the peak was selected (Fig. S1E–F). The points selected through these procedures were defined as “turns” (red points in Fig. S1E–F).

We tested the effect of wind direction and distance from the goal on the occurrence of these turns. First, the number of turns per 160 km in three sections (500–340 km, 340–180 km, and 180–20 km from the goal) were counted. Then, we determined the mean goal direction to the wind; defined as the absolute difference between the mean wind direction and the mean goal direction experienced by the bird or sailboat every 160 km. We fitted "glm" by setting the mean goal direction to the wind (from 0 to π rad) and the section of the movement (three categorical variables 500–340 km, 340–180 km, and 180–20 km) as the explanatory variables, and the number of turns in the 160 km section as the response variable. The log link function and the Poisson distribution were employed. To capture the feature that the number of turns increased with a tailwind and upwind, the square of the mean goal direction to the wind was added to the linear predictor in addition to the average direction of the goal to the wind and the section of the movement.

Model to estimate currency of travel from track data

We constructed a stochastic movement model to clarify what travel currency best explains the albatross movement data. Our model assumed a bird moves with a higher probability in the direction of the greater "travel distance along the goal direction per consumed currency" As described in detail below, this probability was determined by the ground speed of the bird and the rate of consumption of currency, both of which were represented as functions of the travel direction of the bird relative to the wind. The former was a polar diagram already determined, whereas the latter was unknown, and its shape was dependent on the currency of the travel. Our goal was to identify the form of this currency function from experimental data and obtain an implication on the nature of the currency employed by birds. First, we formulated our model and showed that its behavior was determined by the currency function (Step 1). Then, we presented several candidates for the currency function (Step 2). Finally, from the experimental data, we estimated the currency function that best explained the data (Step 3).

[Step 1] formulation of the model

To formulate "travel distance *along the goal direction* per currency", we should first formulate the "travel distance per currency" that is given by dividing the travel speed with CCR (currency consumed per time), i.e.,

$$(\text{travel distance per currency [m]}) = \frac{(\text{distance traveled [m]})}{(\text{currency consumed [ ]})} = \frac{(\text{distance traveled [m]})/(\text{time consumed [s]})}{(\text{currency consumed [ ]})/(\text{time consumed [s]})} = \frac{(\text{travel speed [m s}^{-1}])}{(\text{CCR [s}^{-1}])}.$$

If we denote the travel and goal directions relative to the wind direction at time point t by $\theta_{G,t}$ and $\theta_{P,t}$, then "the travel distance along the goal direction per currency" at time point t is represented as

$$(\text{travel distance along the goal direction per currency})$$

$$= (\text{travel distance per currency}) \times (\cos\theta_{G,t}\cos\theta_{P,t} + \sin\theta_{G,t}\sin\theta_{P,t})$$

$$= \frac{(\text{travel speed}) \times (\cos\theta_{G,t}\cos\theta_{P,t} + \sin\theta_{G,t}\sin\theta_{P,t})}{(\text{CCR })}$$

Hence, by denoting travel distance along the goal direction per currency at time point t as $F(\theta_{G,t}, w_t, \theta_{P,t})$ where w_t represents the wind speed at time point t, the above equation was represented as

$$F(\theta_{G,t}, w_t, \theta_{P,t}, \mathbf{c}) = \frac{V(\theta_{G,t}, w_t)\,(\cos\theta_{G,t}\cos\theta_{P,t} + \sin\theta_{G,t}\sin\theta_{P,t})}{\mathcal{C}(\theta_{G,t}, \mathbf{c})}.$$

The function $V(\theta_{G,t}, w_t)$ represents the travel speed [m s^{-1}] when the birds moved in the direction $\theta_{G,t}$ under wind speed w_t. Here, we used the polar diagram obtained in a previous section as $V(\theta_{G,t}, w_t)$. The function $\mathcal{C}(\theta_{G,t}, \mathbf{c})$ represents the CCR [1/s]. For simplicity, we assumed the CCR only depended on the travel direction of the bird relative to the wind ($\theta_{G,t}$).

Then, we introduced a model whereby the probability distribution of track direction $\theta_{G,t}$, represented as $P(\theta_{G,t})$, was proportional to the exponent of $F(\theta_{G,t})$.

$$P(\theta_{G,t} | w_t, \theta_{P,t}, \mathbf{c}, \beta) = \frac{e^{\beta F(\theta_{G,t}, w_t, \theta_{P,t}, \mathbf{c})}}{Z(w_t, \theta_{P,t}, \mathbf{c}, \beta)},$$

where $Z(w_t, \theta_{P,t}, \mathbf{c}, \beta)$ is the normalizing constant for $\int_{-\pi}^{\pi} P(\theta_{G,t} | w_t, \theta_{P,t}, \mathbf{c}, \beta)\, d\theta_{G,t} = 1$, and is represented as

$$Z(w_t, \theta_{P,t}, \mathbf{c}, \beta) = \int_{-\pi}^{\pi} e^{\beta F(\theta_{G,t}, w_t, \theta_{P,t}, \mathbf{c})}\, d\theta_{G,t}.$$

Our model was formulated by the above equations. The behavior of this model is governed by the functions $V(\theta_{G,t}, w_t)$ and $\mathcal{C}(\theta_{G,t}, \mathbf{c})$. The $V(\theta_{G,t}, w_t)$ is already determined from the experimental data (see **Identification of polar diagram using GAM**). Our goal was to find a currency function $\mathcal{C}(\theta_{G,t}, \mathbf{c})$ that explains the experimental data well.

[Step 2] Formulation of currency consumption functions

The currency function should be able to capture the characteristics of the assumed currency and is ideally simple. Therefore, as the currency function, we employed polynomials up to the second-order of $|\theta_{G,t}|$. We describe the assumed currency for each of the functional forms. Note that we allow only parameters for which the currency function is always positive in $0 \le |\theta_{G,t}| \le \pi$.

For the **constant function**: currency is time,

$$\mathcal{C}(\theta_{G,t}) = 1.$$

The CCR does not change depending on the travel direction. In this case, the currency of travel is time.

For the **linear function**: currency is energy ($c_1 > 0$) or unknown ($c_1 < 0$),

$$\mathcal{C}(\theta_{G,t}) = 1 + c_1|\theta_{G,t}|.$$

When c_1 >0, the CCR increases as the travel direction is upwind. As it is reported that the energy consumption of albatrosses increases as they move upwind (17), when c_1 >0, the currency function is a model that assumes energy as currency. When c_1 <0, however, the CCR decreases as the direction of movement is upwind, and this currency is neither time nor energy.

For the **quadratic function**: currency is unknown,

$$C(\theta_{G,t}) = 1 + c_2(|\theta_{G,t}| - c_3)^2.$$

In this scenario, we assume that c_2 >0. This function minimizes the CCR when the travel direction is toward c_3, and the CCR increases when the travel direction deviates from c_3 in either the upwind or downwind direction.

[Step 3] Stochastic model and calculation of the likelihood from the data

Our goal was to estimate the currency function that best explains natural bird movement data. For this purpose, the likelihood of the model on experimental data should be calculated. We denote the travel direction to the wind, wind speed, and goal direction to the wind at time t obtained from individual i as $\Theta_{G,t}^{(i)}, W_t^{(i)}$, and $\Theta_{P,t}^{(i)}$ (t=1,…, T_i), respectively. In this case, when the observation data is obtained from n individuals, the likelihood is given by

$$L(\boldsymbol{c}, \beta) = \prod_{i=1}^{n} \prod_{t=1}^{T_i} P(\Theta_{G,t}^{(i)} | W_t^{(i)}, \Theta_{P,t}^{(i)}, \mathbf{c}, \beta).$$

Therefore, we computed the BIC for each of the models that employed the currency functions described above and chose the currency function that best explained the data via model selection. The "fminunc" function in MATLAB 2019a was used to calculate the BIC. The normalization constants $Z\left(W_t^{(i)}, \Theta_{P,t}^{(i)}, \mathbf{c}, \beta\right)$ (t=1,…, T_i, i=1,…, N) were computed numerically by Gaussian quadrature with 360 integration points. The estimated values of BIC and parameters for each model are shown in Table S3.

Acknowledgements

The authors thank Chihiro Kinoshita for illustrating the albatross and sailboats in the figures. We thank Masanobu Katori for providing important information about sailing. We thank Vendée Globe for providing the track data of sailboats. We thank the fieldworkers involved in the study on Crozet, and in particular Julien Collet and Alexandre Corbeau. The field work was supported by IPEV (Program 109, PI HW).

Funding

This study was financially supported by the Tohoku Ecosystem Associated Marine Science (TEAMS), Grants-in-Aid for Scientific Research from the Japan Society for the Promotion of Science (15J10905, 24241001, 16H06541, 16H01769, 21H05294, 22H00569), National Geographic (Asia 45-16), and JST CREST Grant Number JPMJCR1685, Japan, and by European Research Council (ERC-2012-ADG_20120314 and ERC-2017-PoC_780058 to HW)

Declaration of interests

The authors declare no competing interests.

References

1. S. A. Shaffer, *et al.*, Migratory shearwaters integrate oceanic resources across the Pacific Ocean in an endless summer. *Proc. Natl. Acad. Sci. U. S. A.* **103**, 12799–12802 (2006).
2. C. Egevang, *et al.*, Tracking of Arctic terns Sterna paradisaea reveals longest animal migration. *Proc. Natl. Acad. Sci. U. S. A.* **107**, 2078–2081 (2010).
3. H. Weimerskirch, M. Salamolard, F. Sarrazin, P. Jouventin, Foraging Strategy of Wandering Albatrosses Through The Breeding Season: A Study Using Satellite Telemetry. *Auk* **110**, 325–342 (1993).
4. Y. Goto, K. Yoda, K. Sato, Asymmetry hidden in birds' tracks reveals wind, heading, and orientation ability over the ocean. *Science advances* (2017).
5. T. Alerstam, Wind as Selective Agent in Bird Migration. *Ornis Scand.* **10**, 76–93 (1979).
6. J. W. Chapman, *et al.*, Animal orientation strategies for movement in flows. *Curr. Biol.* **21**, R861-70 (2011).
7. A. Tarroux, *et al.*, Flexible flight response to challenging wind conditions in a commuting Antarctic seabird: do you catch the drift? *Anim. Behav.* **113**, 99–112 (2016).
8. T. Alerstam, Optimal use of wind by migrating birds: combined drift and overcompensation. *J. Theor. Biol.* **79**, 341–353 (1979).
9. W. J. Richardson, Wind and orientation of migrating birds: a review. *EXS* **60**, 226–249 (1991).
10. S. Åkesson, A. Hedenström, How Migrants Get There: Migratory Performance and Orientation. *Bioscience* **57**, 123–133 (2007).
11. F. Liechti, A. Hedenström, T. Alerstam, Effects of Sidewinds on Optimal Flight Speed of Birds. *J. Theor. Biol.* **170**, 219–225 (1994).
12. E. L. C. Shepard, *et al.*, Energy landscapes shape animal movement ecology. *Am. Nat.* **182**, 298–312 (2013).
13. K. Sato, *et al.*, Scaling of soaring seabirds and implications for flight abilities of giant pterosaurs. *PLoS One* **4**, e5400 (2009).
14. Lord Rayleigh, The soaring of birds. *Nature* **27**, 534–535 (1883).

15. G. K. Taylor, K. V. Reynolds, A. L. R. Thomas, Soaring energetics and glide performance in a moving atmosphere. *Philos. Trans. R. Soc. Lond. B Biol. Sci.* **371** (2016).
16. G. D. Bousquet, M. S. Triantafyllou, J.-J. E. Slotine, Optimal dynamic soaring consists of successive shallow arcs. *J. R. Soc. Interface* **14** (2017).
17. H. Weimerskirch, T. Guionnet, J. Martin, S. A. Shaffer, D. P. Costa, Fast and fuel efficient? Optimal use of wind by flying albatrosses. *Proc. Biol. Sci.* **267**, 1869–1874 (2000).
18. P. L. Richardson, How do albatrosses fly around the world without flapping their wings? *Prog. Oceanogr.* **88**, 46–58 (2011).
19. P. L. Richardson, E. D. Wakefield, R. A. Phillips, Flight speed and performance of the wandering albatross with respect to wind. *Mov Ecol* **6**, 3 (2018).
20. P. Jouventin, H. Weimerskirch, Satellite tracking of Wandering albatrosses. *Nature* **343**, 746–748 (1990).
21. H. Weimerskirch, *et al.*, GPS tracking of foraging albatrosses. *Science* **295**, 1259 (2002).
22. H. Weimerskirch, Linking demographic processes and foraging ecology in wandering albatross-Conservation implications. *J. Anim. Ecol.* **87**, 945–955 (2018).
23. T. Alerstam, G. A. Gudmundsson, B. Larsson, Flight tracks and speeds of Antarctic and Atlantic seabirds: radar and optical measurements. *Philos. Trans. R. Soc. Lond. B Biol. Sci.* **340**, 55–67 (1993).
24. L. B. Spear, D. G. Ainley, Flight behaviour of seabirds in relation to wind direction and wing morphology. *Ibis* (1997) https:/doi.org/10.1111/j.1474-919X.1997.tb04620.x.
25. G. A. Nevitt, M. Losekoot, H. Weimerskirch, Evidence for olfactory search in wandering albatross, Diomedea exulans. *Proc. Natl. Acad. Sci. U. S. A.* **105**, 4576–4581 (2008).
26. F. Ventura, J. P. Granadeiro, O. Padget, P. Catry, Gadfly petrels use knowledge of the windscape, not memorized foraging patches, to optimize foraging trips on ocean-wide scales. *Proc. Biol. Sci.* **287**, 20191775 (2020).
27. F. Ventura, *et al.*, A central place foraging seabird flies at right angles to the wind to jointly optimize locomotor and olfactory search efficiency. *Proc. Biol. Sci.* **289**, 20220895 (2022).
28. G. H. Orians, N. E. Pearson, On the theory of central place foraging. Analysis of ecological systems. *Ohio State University Press, Columbus* (1979).
29. E. D. Wakefield, *et al.*, Wind field and sex constrain the flight speeds of central-place foraging albatrosses. *Ecol. Monogr.* **79**, 663–679 (2009).

30. H. Weimerskirch, Are seabirds foraging for unpredictable resources? *Deep Sea Res. Part 2 Top. Stud. Oceanogr.* **54**, 211–223 (2007).

31. J. A. Kempton, *et al.*, Optimization of dynamic soaring in a flap-gliding seabird affects its large-scale distribution at sea. *Sci Adv* **8**, eabo0200 (2022).

32. H. Weimerskirch, D. Pinaud, F. Pawlowski, C.-A. Bost, Does prey capture induce area-restricted search? A fine-scale study using GPS in a marine predator, the wandering albatross. *Am. Nat.* **170**, 734–743 (2007).

33. A. Corbeau, J. Collet, M. Fontenille, H. Weimerskirch, How do seabirds modify their search behaviour when encountering fishing boats? *PLoS One* **14**, e0222615 (2019).

34. P. J. Richards, A. Johnson, A. Stanton, America’s Cup downwind sails—vertical wings or horizontal parachutes? *J. Wind Eng. Ind. Aerodyn.* **89**, 1565–1577 (2001).

35. R. Stelzer, T. Pröll, Autonomous sailboat navigation for short course racing. *Rob. Auton. Syst.* **56**, 604–614 (2008).

36. R. M. Johnstone, L. S. Davis, Incubation routines and foraging-trip regulation in the Grey-faced Petrel Pterodroma macroptera gouldi. *Ibis* (1990) https:/doi.org/10.1111/j.1474-919X.1990.tb01011.x.

37. H. Weimerskirch, Regulation of foraging trips and incubation routine in male and female wandering albatrosses. *Oecologia* **102**, 37–43 (1995).

38. R. McNeill Alexander, *Principles of Animal Locomotion* (Princeton University Press, 2003).

39. C. J. Pennycuick, M. J. Lighthill, The flight of petrels and albatrosses (procellariiformes), observed in South Georgia and its vicinity. *Philos. Trans. R. Soc. Lond. B Biol. Sci.* **300**, 75–106 (1982).

40. G. Sachs, In-flight measurement of upwind dynamic soaring in albatrosses. *Prog. Oceanogr.* **142**, 47–57 (2016).

41. Y. Yonehara, *et al.*, Flight paths of seabirds soaring over the ocean surface enable measurement of fine-scale wind speed and direction. *Proc. Natl. Acad. Sci. U. S. A.* **113**, 9039–9044 (2016).

42. N. Horvitz, *et al.*, The gliding speed of migrating birds: slow and safe or fast and risky? *Ecol. Lett.* **17**, 670–679 (2014).

43. R. Harel, *et al.*, Decision-making by a soaring bird: time, energy and risk considerations at different spatio-temporal scales. *Philos. Trans. R. Soc. Lond. B Biol. Sci.* **371** (2016).

44. W. M. G. Vansteelant, J. Shamoun-Baranes, J. McLaren, J. van Diermen, W. Bouten, Soaring across continents: decision-making of a soaring migrant under

changing atmospheric conditions along an entire flyway. *J. Avian Biol.* **48**, 887–896 (2017).

45. C. J. Pennycuick, *Modelling the Flying Bird* (Elsevier, 2008).

46. Z. Akos, M. Nagy, T. Vicsek, Comparing bird and human soaring strategies. *Proc. Natl. Acad. Sci. U. S. A.* **105**, 4139–4143 (2008).

47. G. Sachs, Minimum shear wind strength required for dynamic soaring of albatrosses. *Ibis* **147**, 1–10 (2005).

48. Y. Goto, K. Yoda, H. Weimerskirch, K. Sato, How did extinct giant birds and pterosaurs fly? A comprehensive modeling approach to evaluate soaring performance. *PNAS Nexus* (2022) https:/doi.org/10.1093/pnasnexus/pgac023.

49. R. B. Stull, *An Introduction to Boundary Layer Meteorology* (Springer Science & Business Media, 1988).

50. A. Bernard, A. S. L. Rodrigues, V. Cazalis, D. Grémillet, Toward a global strategy for seabird tracking. *Conserv. Lett.* **14** (2021).

51. E. Lempidakis, *et al.*, Pelagic seabirds reduce risk by flying into the eye of the storm. *Proc. Natl. Acad. Sci. U. S. A.* **119**, e2212925119 (2022).

52. E. Nourani, *et al.*, Extreme tolerable winds for seabirds are determined by morphology. *bioRxiv*, 2022.05.02.490292 (2022).

53. C. Pêtrès, M.-A. Romero-Ramirez, F. Plumet, A potential field approach for reactive navigation of autonomous sailboats. *Rob. Auton. Syst.* **60**, 1520–1527 (2012).

54. H. Saoud, M.-D. Hua, F. Plumet, F. Ben Amar, Routing and course control of an autonomous sailboat in *2015 European Conference on Mobile Robots (ECMR)*, (ieeexplore.ieee.org, 2015), pp. 1–6.

55. F. Bonadonna, *et al.*, Orientation in the wandering albatross: interfering with magnetic perception does not affect orientation performance. *Proc. Biol. Sci.* **272**, 489–495 (2005).

56. C. Girard, S. Benhamou, L. Dagorn, FAD: Fish Aggregating Device or Fish Attracting Device? A new analysis of yellowfin tuna movements around floating objects. *Anim. Behav.* **67**, 319–326 (2004).

57. S. N. Wood, *Generalized additive models: an introduction with R* (chapman and hall/CRC, 2006).